Guided elastic waves at a periodic array of thin coplanar cavities in a solid

A. G. Every
School of Physics, University of the Witwatersrand, P.O. Wits 2050, South Africa
(Received 9 August 2008; published 6 November 2008)

This paper is concerned with guided elastic waves at a periodic array of thin coplanar cavities in a solid and the role they play in the scattering of incident longitudinal and transverse waves in the plane perpendicular to the cavities. It is treated as a mixed boundary-condition plane strain problem pertaining to two elastic half spaces which are joined together within infinitely long regularly spaced strips and unattached in between. It provides an approach to modeling wave interactions at an array of coplanar cracks, partially bonded surfaces, mining stopes, and other analogous physical situations, and it is of relevance in the topical field of phononic crystals. The method of analysis brought to bear on this problem involves smoothing out the discontinuities in the boundary conditions, invoking a truncated Fourier series representation of the wave field and applying the boundary conditions at a discrete set of points within the repeat interval at the interface to determine the Fourier coefficients. The dispersion relation for interfacial waves is obtained, and it is shown how (in the supersonic domain with respect to bulk transverse waves) there are branches associated with leaky interfacial waves, which at certain isolated points in k space uncouple from the bulk wave continuum to exist as secluded supersonic interfacial waves. These observations are able to explain striking resonant features in the scattering of bulk waves at the interface.

DOI: 10.1103/PhysRevB.78.174104 PACS number(s): 62.30.+d, 43.20.+g

I. INTRODUCTION

This paper is concerned with guided elastic waves at a periodic array of thin coplanar cavities in an isotropic elastic solid and the way in which leaky supersonic branches of these modes are featured in the scattering of bulk elastic waves. It is framed as a mixed boundary-condition (BC) problem[1] pertaining to two half spaces sharing a planar interface, where they are joined together within infinitely long regularly spaced strips and unattached in between. In the continuum mechanics community this is regarded as the problem of wave scattering by a periodic array of thin coplanar cracks, and there is an extensive literature on it and related problems.[2–15] It is, however, a paradigm for a much broader range of physical situations giving rise to elastic wave scattering, including solids with slightly uneven surfaces which are in contact, buried interdigital structures that might be used for signal processing, and stoping in mine operations, where a narrow seam of mineral is removed, leaving regularly positioned pillars for roof support. In light of the current widespread interest in phononic crystals,[16,17] and in scattering from corrugated surfaces,[17] it would seem an opportune moment to revisit this problem. It provides a somewhat different perspective from the prevailing emphasis in these fields in that it deals not with the periodic variation of bulk properties or surface profiles but with the periodic variation of boundary conditions. Mixed boundary-condition problems are considered to be particularly challenging,[1] especially where there are discontinuities in the boundary conditions,[18] and in regard to their application to cracks, they have elicited sophisticated methods for their solution.[2–15] The method of analysis brought to bear on this problem here involves smoothing over the discontinuities in the boundary conditions, invoking a truncated Fourier series representation for the wave field, and applying the boundary conditions at a discrete set of points within the repeat interval at the interface to determine the Fourier coefficients. While not optimally suited for establishing formal results such as, e.g., the asymptotic form of the dynamic strain field near a crack tip, it is conceptually simpler than hitherto adopted approaches. It is a reliable, practical method for interpreting information that is accessible to ultrasonic probing and is able to accurately reproduce published numerical results obtained by other more elaborate methods, including the extensive set of transmission and reflection curves reported by Mikata,[5] which were obtained by a singular integral equation approach and the use of a Chebychev polynomial expansion. Venturing into a different terrain in the present paper, the dispersion relation for interfacial waves (IWs) is obtained within a one-dimensional folded Brillouin-zone scheme, and it is shown how [in the supersonic domain with respect to bulk transverse (T) waves] there are branches associated with leaky interfacial waves, which at certain isolated points in wave-vector space uncouple from the bulk wave continuum to exist as secluded supersonic interfacial waves (SSIW). These observations are able to explain striking resonant features in the scattering of bulk waves at the interface, some of which have been noted before in the literature[3,5,7] but not explained in any depth. Light scattering,[19,20] the optical pump probe technique,[21] and the laser transient grating technique,[22] which have been used for studying hybridized guided acoustic modes at surface gratings, could provide means for observing the interfacial modes discussed here.

II. DESCRIPTION OF MODEL AND METHOD OF ANALYSIS

Figure 1 depicts the physical situation treated in this paper. Two identical semi-infinite solids occupy the half spaces on opposite sides of the $z=0$ plane. They are perfectly bonded to each other within regularly spaced infinitely long strips parallel to the y axis, each of width b in the x direction.

 ©2008 The American Physical Society

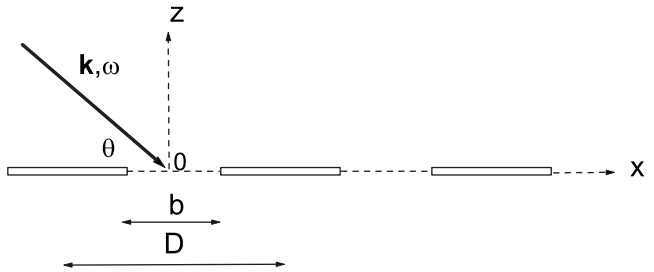

FIG. 1. Incidence of a homogeneous plane wave on a periodically joined interface between two identical elastic half spaces. The surfaces of the solids are joined within strips of width b and free in between, and the repeat distance is D.

Between the strips, within the cracks as it were, the surfaces of the two solids are completely free. The repeat distance of this arrangement in the x direction is D. A plane longitudinal (L) or sagittally (SV) polarized T wave of wave vector $\mathbf{k}=(k_x,k_z)$ and angular frequency ω is incident on the interface at an angle θ as shown, giving rise to scattering. This constitutes a plane strain problem in which the displacement field $\mathbf{u}(x,z)\exp(-i\omega t)$ is confined to the xz plane and is independent of y. The somewhat simpler antiplane strain problem of scattering of shear horizontal (SH) y-polarized waves, which has been treated by a number of authors,[4,11,13,14,23,24] will not be dealt with here.

The solids are of density ρ, and Lamé elastic constants λ and μ, with their L and T acoustic slownesses (inverse phase velocities) being given, respectively, by[25]

$$\alpha = 1/V_L = \sqrt{\rho/(\lambda + 2\mu)}, \tag{1a}$$

$$\beta = 1/V_T = \sqrt{\rho/\mu}. \tag{1b}$$

The ratio of the two slownesses is

$$\frac{\alpha}{\beta} = \sqrt{\frac{(1-2\nu)}{2(1-\nu)}}, \tag{2}$$

where ν is Poisson's ratio. Most of the calculations reported below are for the physically typical value of $\nu=0.3$, but a consequence of ν being negative will be discussed. The relevant components of the stress (σ_{ij})-strain $[\varepsilon_{ij}=\frac{1}{2}(\frac{\partial u_i}{\partial x_j}+\frac{\partial u_j}{\partial x_i})]$ relationship that arise in the application of the boundary conditions are

$$\sigma_{zz} = \lambda(\varepsilon_{zz} + \varepsilon_{xx}) + 2\mu\varepsilon_{zz}, \tag{3a}$$

$$\sigma_{xz} = 2\mu\varepsilon_{xz}. \tag{3b}$$

The scattered field at infinity is required to conform to the Sommerfeld radiation conditions.[1,25] At the interface the combined incident and scattered fields is required to satisfy the BCs of continuity of displacements and traction forces within the joined regions, and the vanishing of traction forces within the unattached regions.[1,25] In order to obtain dimensionally equivalent equations from these two types of BCs, the tractions are defined here as

$$t_{xz}(0_\pm) = \frac{\beta}{\rho\omega}\sigma_{xz}(0_\pm), \tag{4a}$$

$$t_{zz}(0_\pm) = \frac{\beta}{\rho\omega}\sigma_{zz}(0_\pm). \tag{4b}$$

The BCs can then be expressed as follows:

$$t_{xz}(0_-) = t_{xz}(0_+), \tag{5a}$$

$$t_{zz}(0_-) = t_{zz}(0_+), \tag{5b}$$

throughout the attached and unattached regions,

$$u_x(0_+) - u_x(0_-) = 0, \tag{5c}$$

$$u_z(0_+) - u_z(0_-) = 0, \tag{5d}$$

in the joined regions, and

$$t_{xz}(0_+) = 0, \tag{5e}$$

$$t_{zz}(0_+) = 0, \tag{5f}$$

in the unattached regions. It is assumed, subject to the qualifying remarks below, that the wave amplitude is sufficiently small and there is a large enough gap between the free surfaces that these surfaces are not brought into contact through the wave motion. Maugin *et al.*[10,11] treated the case of cracks for which the surfaces are in contact but able to slip by setting the shear stress at the interface to be proportional to the relative displacement of the two surfaces. Variants of such modified boundary conditions have in fact been quite widely used over the years to model imperfect bonding between solids (see, e.g., Refs. 25–28).

For the present problem, there are advantages to formulating a unified set of position-dependent BCs that apply everywhere at the interface by combining, respectively, Eqs. (5c) and (5e) and Eqs. (5d) and (5f) in the following way:

$$\frac{\eta(x)}{2}[u_x(0_+) - u_x(0_-)] - [1 - \eta(x)]t_{xz}(0_\pm) = 0, \tag{5g}$$

$$\frac{\eta(x)}{2}[u_z(0_+) - u_z(0_-)] - [1 - \eta(x)]t_{zz}(0_\pm) = 0, \tag{5h}$$

where $0 \le \eta(x) \le 1$, with $\eta(x)=1$ in the joined regions and $\eta(x)=0$ in the unattached regions. The ratio $\eta(x)/[1-\eta(x)]$ represents the "degree of attachment" of the two solids, which is infinite for perfect joining and zero for total detachment. By allowing $\eta(x)$ to vary continuously between 1 and 0 over a small smoothing interval separating the joined and unattached regions, one can model, for example, a crack tip which is somewhat diffuse in nature as a consequence of the material being weakened by plastic deformation just in front of the crack tip,[29] and there are possibly still some interaction between the cleaved surfaces just behind the crack tip. In this way one can sidestep difficult issues concerning the precise shape of the crack tip[30] and finite wave amplitude, for which there may be a region close to the crack tip where the opposing surfaces periodically collide and part, giving

rise to nonlinear effects.[31,32] Likewise, where one is considering scattering by cavities of small but finite thickness at the interface, as in the case of mine stopes,[33] this provides a way of avoiding complications associated with the detailed shape of the edges of the cavities. This smoothing of $\eta(x)$ has significant analytical and numerical advantages, too, of giving one the control over the convergence of the Fourier series expansion of the wave field and avoiding unphysical singular behavior predicted by linear elasticity at discontinuities in boundary conditions.[18] In the calculations below, $\eta(x)$ is taken to have the form

$$\eta(x) = \frac{1}{2}\left[\mathrm{Erf}\left(\frac{x+b/2}{d}\right) - \mathrm{Erf}\left(\frac{x-b/2}{d}\right)\right]; \quad \frac{-D}{2} < x < \frac{D}{2}, \tag{6}$$

where Erf is the error function. This locates the joined region, of width b, in the center of the repeat interval $-D/2 < x < D/2$ and describes a smoothing over interval between the joined and unattached regions of width $\approx 2d$. There does not appear to have been any widespread use in the past of this type of approach to smoothing out boundary-condition discontinuities.[34] In the analysis that follows, the boundary conditions (5a), (5b), (5g), and (5h) are employed in determining scattered fields and guided modes.

The physical situation being considered here has reflection symmetry through the $z=0$ plane, and this allows one to treat separately the wave fields which are symmetric and antisymmetric with respect to reflection through this plane.[3] For the symmetric field, u_x is the same on the two sides of the interface and u_z points in opposite directions, while for the antisymmetric field, it is u_z that is the same on the two sides of the interface and it is u_x that points in opposite directions. An incoming plane wave from one side and its resultant scattered field is then taken as the superposition of symmetrically and antisymmetrically disposed pairs of incoming waves and their scattered fields.

A. Symmetric field

Consider a pair of symmetrically incident unit amplitude plane homogeneous L waves of angular frequency ω and wave vectors $(k_x, \pm k_z^{\alpha 0})$, with the minus sign pertaining to the wave in the upper half space and the plus sign to the one in the lower half space. The angle of incidence with respect to the interface is given by

$$\cos\theta = k_x/k; \quad k^2 = \omega^2\alpha^2 = (k_x)^2 + (k_z^{\alpha 0})^2. \tag{7}$$

As a consequence of the discrete rather than continuous translational invariance of the boundary conditions in the x direction, k_x is preserved in the scattered field only to within an integral multiple of the reciprocal lattice vector $2\pi/D$ associated with the periodicity of the interface, and so the scattered field is a superposition of an infinite number of Bloch harmonics, i.e., outgoing L and sagittally polarized T waves of the same frequency and with wave vectors $(k_x^n, \pm k_z^{\alpha n})$ and $(k_x^n, \pm k_z^{\beta n})$, respectively, where

$$k_x^n = k_x + 2\pi n/D; \quad n = 0, \pm 1, \pm 2, \ldots, \tag{8a}$$

$$k_z^{\alpha n} = \sqrt{\omega^2\alpha^2 - (k_x^n)^2}, \tag{8b}$$

$$k_z^{\beta n} = \sqrt{\omega^2\beta^2 - (k_x^n)^2}. \tag{8c}$$

The absolute magnitudes of the k's are thereby $\omega\alpha$ for the L partial waves and $\omega\beta$ for the T partial waves. Depending on the value of ω and k_x, some of the $k_z^{\alpha n}$ and $k_z^{\beta n}$ are real, and the remaining are imaginary. The choice of sign $(\pm)$ is dictated by the Sommerfeld conditions[1,25] that in the case of a homogeneous wave, i.e., k_z real, the wave should be directed away from the interface, and in the case of an inhomogeneous wave, i.e., k_z imaginary, the wave should be evanescent, i.e., fall off exponentially away from the interface. To start with, for small ω, there will be only one outgoing homogeneous L and one outgoing homogeneous T wave in each half space, with the rest of the partial waves being evanescent. As ω is increased, successive critical values or thresholds are crossed, where an evanescent wave converts to homogeneous.

The wave fields in the upper and lower half spaces for a symmetrically incident L wave are, thus,

$$\mathbf{u} = \frac{1}{\alpha\omega}(k_x, -k_z^{\alpha 0})e^{i(k_x x - k_z^{\alpha 0} z)} + \sum_n \left\{ A_n \frac{1}{\alpha\omega}(k_x^n, k_z^{\alpha n})e^{i(k_x^n x + k_z^{\alpha n} z)} + B_n \frac{1}{\beta\omega}(-k_z^{\beta n}, k_x^n)e^{i(k_x^n x + k_z^{\beta n} z)} \right\}; \quad z > 0, \tag{9a}$$

$$\mathbf{u} = \frac{1}{\alpha\omega}(k_x, k_z^{\alpha 0})e^{i(k_x x + k_z^{\alpha 0} z)} + \sum_n \left\{ A_n \frac{1}{\alpha\omega}(k_x^n, -k_z^{\alpha n})e^{i(k_x^n x - k_z^{\alpha n} z)} + B_n \frac{1}{\beta\omega}(-k_z^{\beta n}, -k_x^n)e^{i(k_x^n x - k_z^{\beta n} z)} \right\}; \quad z < 0. \tag{9b}$$

There is an implicit time-dependent factor $e^{-i\omega t}$ in all the wave expressions presented here, which is concealed for the sake of brevity. The first terms in Eqs. (9a) and (9b) pertain to the incident field and the summed terms to the scattered field. The quantities $\frac{1}{\alpha\omega}(k_x^n, k_z^{\alpha n})$ and $\frac{1}{\beta\omega}(k_z^{\beta n}, k_x^n)$, etc., are unit polarization vectors for the partial waves. For a symmetrically incident T wave, the first terms in Eqs. (9a) and (9b) are replaced, respectively, by $\frac{1}{\beta\omega}(-k_z^{\beta 0}, -k_x^0)e^{i(k_x^0 x - k_z^{\beta 0} z)}$ and $\frac{1}{\beta\omega}(-k_z^{\beta 0}, k_x^0)e^{i(k_x^0 x + k_z^{\beta 0} z)}$.

A numerical solution to this problem is obtained by imposing a finite cutoff on the expansion, limiting n to the range $-N \le n \le N$, where N is a suitably large integer. The numerical results reported in this paper are for $N=47$, which provides sufficient accuracy, but calculations have been carried out for several different values of N ranging from 17 to 67, and it has been found that toward the higher end of this range the slight gain in accuracy does not justify the rapid increase in computational time. The values of the $2N+1$ coefficients A_n, and equal number of B_n, are determined by imposing the boundary conditions (5a), (5b), (5g), and (5h) at a discrete set of $2N+1$ equally spaced points $x_p = pD/(2N+1)$; $p = 0, \pm 1, \ldots \pm N$ in the interval $-D/2 < x_p < D/2$. Angel and Achenbach[3] started off in a similar way with a finite Fourier series but then reduced it to a singular integral equation, which they solved numerically.

Digitization of boundary conditions in this way was employed by Castaings *et al.*[35] in modeling the interaction of Lamb waves with a crack in a plate.

As a consequence of the symmetry of the wave field under reflection through the $z=0$ plane, $t_{zz}(0_+)=t_{zz}(0_-)$, and so BC (5b) is automatically satisfied throughout the interval without yielding any conditions on A_n and B_n. Next, the symmetry of the field implies that $t_{xz}(0_+)=-t_{xz}(0_-)$, and it follows then from BC (5a) that $t_{xz}(0_+)=0$. Imposing this condition on Eq. (9a) yields

$$\sum_n \{2(A_n-\delta_{n0})k_x^n k_z^{\alpha n}-B_n[\omega^2\beta^2-2(k_x^n)^2]\}\exp\left(i\frac{2\pi n}{D}x_p\right)=0;\quad p=0,\pm 1,\ldots,\pm N. \tag{10}$$

Equation (10) can be regarded as the finite Fourier series expansion of a function which is zero throughout the interval $-D/2<x_p<D/2$, and hence all the coefficients in this series, i.e., the quantities in braces, are zero. This allows B_n to be expressed in terms of A_n; thus,

$$B_n=\frac{2(A_n-\delta_{n0})k_x^n k_z^{\alpha n}}{[\omega^2\beta^2-2(k_x^n)^2]}. \tag{11}$$

For a symmetrically incident T wave, the corresponding result is

$$B_n=\frac{2A_n k_x^n k_z^{\alpha n}}{[\omega^2\beta^2-2(k_x^n)^2]}+\delta_{n0}. \tag{12}$$

A further consequence of the symmetry of the wave field is that $u_x(0_+)=u_x(0_-)$, which through BC (5g) again implies $t_{xz}(0_+)=0$, thereby not yielding any new constraint on the coefficients. Finally, from BC (5h), and after eliminating B_n using Eq. (11) or (12), one arrives at a set of $2N+1$ equations determining A_n,

$$\sum_{n=-N}^{N} M_{pn}A_n=m_p;\quad p=0,\pm 1,\ldots,\pm N, \tag{13}$$

where, for a symmetrically incident L wave,

$$M_{pn}=\left\{\eta(x_p)\left\{\frac{k_z^{\alpha n}\omega\beta}{[\omega^2\beta^2-2(k_x^n)^2]}\right\}-i[1-\eta(x_p)]\times\left\{\frac{[\omega^2\beta^2-2(k_x^n)^2]^2+4(k_x^n)^2k_z^{\alpha n}k_z^{\beta n}}{[\omega^2\beta^2-2(k_x^n)^2]\omega^2\beta^2}\right\}\right\}\times\exp\left(i\frac{2\pi n}{D}x_p\right), \tag{14}$$

and

$$m_p=\left\{\eta(x_p)\left\{\frac{k_z^{\alpha 0}\omega\beta}{[\omega^2\beta^2-2(k_x^0)^2]}\right\}-i[1-\eta(x_p)]\times\left\{\frac{4(k_x^0)^2k_z^{\alpha 0}k_z^{\beta 0}-[\omega^2\beta^2-2(k_x^0)^2]^2}{[\omega^2\beta^2-2(k_x^0)^2]\omega^2\beta^2}\right\}\right\}. \tag{15}$$

For a symmetrically incident T wave, M_{pn} is the same, i.e., given by Eq. (14), but m_p is given by

$$m_p=\left\{i[1-\eta(x_p)]\left(\frac{4k_x^0k_z^{\beta 0}}{\omega^2\beta^2}\right)\right\}. \tag{16}$$

The solution of Eq. (13),

$$A_n=(M^{-1})_{np}m_p, \tag{17}$$

yields the amplitudes A_n, and substitution into Eq. (11) or (12) then yields B_n for the symmetrical field.

B. Antisymmetric field

For an antisymmetrically incident pair of L waves, the field in the upper half space is given, as before, by Eq. (9a), while the field in the lower half space is the negative of Eq. (9b). Again one determines the values of the $2N+1$ coefficients $\tilde{A}_n$ and equal number of $\tilde{B}_n$ (a tilde has been used to distinguish these coefficients from the previous ones) by imposing the boundary conditions at the same discrete set of points.

As a consequence of the antisymmetry of the wave field under reflection through the $z=0$ plane, $t_{xz}(0_+)=t_{xz}(0_-)$, and so BC (5a) is automatically satisfied throughout the interval without yielding any conditions on $\tilde{A}_n$ and $\tilde{B}_n$. Next, the antisymmetry of the field implies that $t_{zz}(0_+)=-t_{zz}(0_-)$, and it follows then from BC (5b) that $t_{zz}(0_+)=0$. Imposing this condition on Eq. (9a) yields

$$\sum_n \{(\tilde{A}_n+\delta_{n0})[\omega^2\beta^2-2(k_x^n)^2]+2\tilde{B}_n k_x^n k_z^{\beta n}\}\exp\left(i\frac{2\pi n}{D}x_p\right)=0;\quad p=0,\pm 1,\ldots,\pm N, \tag{18}$$

which (as before) can be regarded as the finite Fourier series expansion of a function which is zero throughout the interval, and hence all the coefficients in this series are zero. This allows $\tilde{B}_n$ to be expressed in terms of $\tilde{A}_n$; thus,

$$\tilde{B}_n=-\frac{(\tilde{A}_n+\delta_{n0})[\omega^2\beta^2-2(k_x^n)^2]}{2k_x^n k_z^{\beta n}}. \tag{19}$$

For an antisymmetrically incident T wave, the corresponding result is

$$\tilde{B}_n=-\frac{\tilde{A}_n[\omega^2\beta^2-2(k_x^n)^2]}{2k_x^n k_z^{\beta n}}-\delta_{n0}. \tag{20}$$

A further consequence of the antisymmetry of the field is that $u_z(0_+)=u_z(0_-)$, which through BC (5h) again implies $t_{zz}(0_+)=0$ (not providing any new constraint on the coefficients). Finally from BC (5g), and after eliminating $\tilde{B}_n$ using Eq. (19) or (20), one arrives at a set of $2N+1$ equations determining $\tilde{A}_n$,

$$\sum_{n=-N}^{N} \tilde{M}_{pn}\tilde{A}_n=\tilde{m}_p;\quad p=0,\pm 1,\ldots,\pm N, \tag{21}$$

where

$$\tilde{M}_{pn} = \left\{ \eta(x_p)\left[\frac{\omega\beta}{k_x^n}\right] - i[1-\eta(x_p)] \times \left\{ \frac{[\omega^2\beta^2 - 2(k_x^n)^2]^2 + 4(k_x^n)^2 k_z^{\alpha n} k_z^{\beta n}}{k_x^n k_z^{\beta n}\omega^2\beta^2} \right\} \right\} \exp\left(i\frac{2\pi n}{D}x_p\right) \tag{22}$$

and

$$\tilde{m}_p = \left\{ -\eta(x_p)\left[\frac{\omega\beta}{k_x^0}\right] + i[1-\eta(x_p)] \times \left\{ \frac{[\omega^2\beta^2 - 2(k_x^0)^2]^2 + 4(k_x^0)^2 k_z^{\alpha 0} k_z^{\beta 0}}{k_x^0 k_z^{\beta 0}\omega^2\beta^2} \right\} \right\}. \tag{23}$$

For an antisymmetrically incident T wave $\tilde{M}_{pn}$ is the same, i.e., given by Eq. (22), but $\tilde{m}_p$ is given by

$$\tilde{m}_p = \left\{ +i[1-\eta(x_p)] \left\{ \frac{4[\omega^2\beta^2 - 2(k_x^0)^2]}{\omega^2\beta^2} \right\} \right\}. \tag{24}$$

The solution of Eq. (21),

$$\tilde{A}_n = (\tilde{M}^{-1})_{np}\tilde{m}_p, \tag{25}$$

yields the amplitudes $\tilde{A}_n$, and substitution into Eq. (19) or (20) then yields $\tilde{B}_n$ for the antisymmetrical field.

III. INTERFACIAL WAVES

The matrices M and $\tilde{M}$ become singular under certain conditions, leading to the existence of Stoneley-type IW, i.e., subsonic guided waves in the spectral range $0<\omega<k/\beta$, and contained within the first zone of the folded Brillouin-zone scheme, i.e., $0<k_x<\pi/D$, which consists entirely of evanescent partial-wave components that satisfy the boundary conditions. These modes are conditioned on the vanishing of $\det(M)$ or $\det(\tilde{M})$. In the supersonic domain, there occur near singular features associated with pseudointerfacial waves (PIW). Figure 2(a) is a plot, for the symmetrical mode, of $\log[|\det(M)|]$ versus dimensionless frequency $\hat{\omega}=\omega\beta D/\pi$ near the $n=0$ and -1 T wave thresholds T_0 and T_{-1}, respectively, and calculated for $\nu=0.3$, $b/D=0.35$, and fixed value of the reduced wave number $\hat{k}_x=k_xD/\pi=0.99$, which is close to the Brillouin-zone edge. It displays an IW singularity at $\hat{\omega}=0.9676$, denoted as IW(S). The kinks at $\hat{\omega}=0.99$ and 1.01 correspond, respectively, to the T_0 and T_{-1} thresholds at which these modes convert from evanescent to homogeneous with increasing frequency.

Figure 2(b) shows a similar plot for the antisymmetrical mode of $\log[|\det(\tilde{M})|]$ versus $\hat{\omega}$ for fixed $\hat{k}_x=0.85$. It displays an IW singularity at $\hat{\omega}=0.829$, denoted as IW(A), sharp maxima at $\hat{\omega}=0.85$ and 1.15 which correspond, respectively, to the T_0 and T_{-1} thresholds, and a sharp but nonsingular minimum at $\hat{\omega}=1.117$, denoted as PIW(A), which is associated with a pseudointerfacial wave. The last mentioned is a mode that consists predominantly of evanescent partial-wave components but, through a weak coupling to the $n=0$ T bulk wave continuum, is a leaky rather than perfect guided mode.

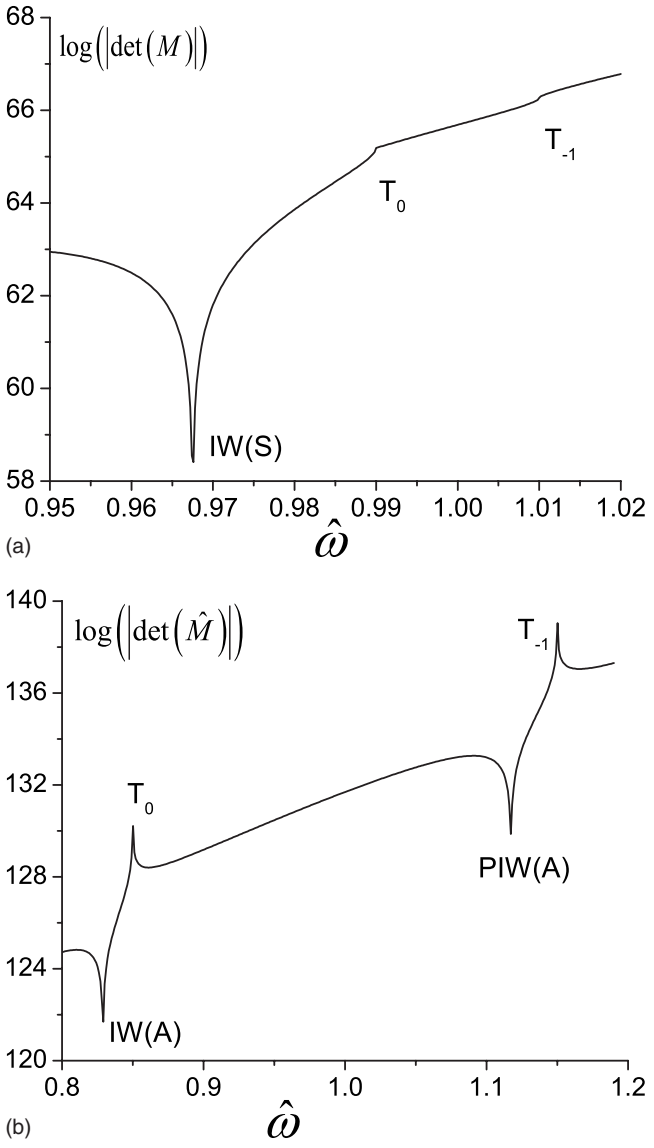

FIG. 2. (a) Plot for the symmetric mode of $\log[|\det(M)|]$ versus $\hat{\omega}$ for $\hat{k}_x=0.99$. (b) Plot for the antisymmetric mode of $\log[|\det(\tilde{M})|]$ versus $\hat{\omega}$ for fixed $\hat{k}_x=0.85$. The calculations are based on $\nu=0.3$, $b/D=0.35$, $d/D=0.02$, and $N=47$.

It features, as we will see, importantly in the scattering of bulk waves at the interface.

Figures 2(a) and 2(b) have been calculated for $N=47$ and the smoothing parameter has been set at $d/D=0.02$, which is small enough that $\eta(x)$ deviates significantly from zero and unity in no more than about 5% of the interval $-D/2<x<D/2$ but large enough that A_n, $\tilde{A}_n$, B_n, and $\tilde{B}_n$ have fallen to less than about 1% of their maximum values for n approaching $\pm N$. Reducing d further has the effect of shifting the IW and PIW very slightly upward in frequency but without altering (in essence) their nature, and the threshold features are unaffected. In the limit $d\to 0$, i.e., for perfectly sharp borders between the bonded and free-surface regions, A_n and other coefficients tend (with increasing n) to alternate in absolute value, not converging to zero but approaching a mean value of about 0.2 as $n\to\pm N$; however,

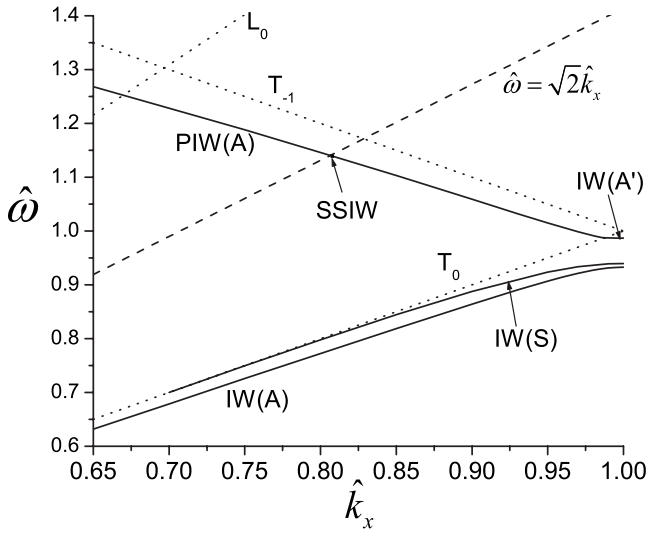

FIG. 3. Dispersion relation for the IW and PIW near the Brillouin-zone boundary for $\nu=0.3$, $b/D=0.16$, $d/D=0$, and $N=47$. It shows also the thresholds T_0, T_{-1}, and L_0, which are independent of the value of b. IW(A) persists down to $\hat{k}_x=0$, approaching asymptotically to the T_0 threshold at this lower limit.

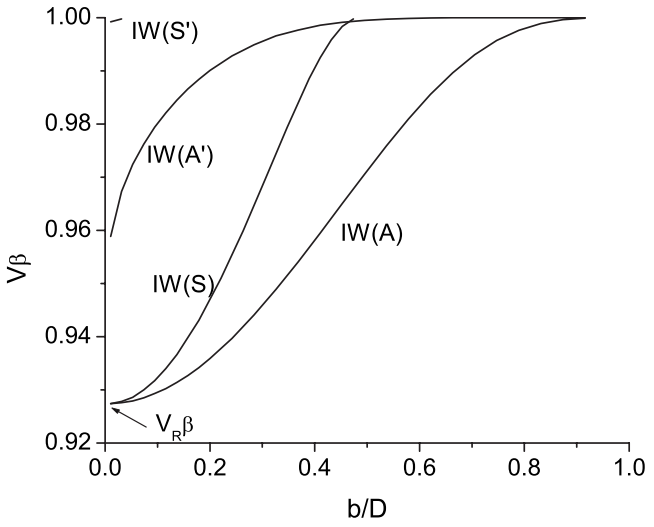

FIG. 4. Standing mode phase velocities at the zone boundary $\hat{k}_x=1$ as a function of b/D for $\nu=0.3$, $d/D=0$, and $N=47$.

large N is taken. That they do not converge to zero for large N is attributable to the fact that for d that is less than the discretization interval, the width of the smoothing interval is effectively dictated by the value of $D/(2N+1)$ and not by d. As N is increased, the borders become sharper, and the number of Fourier terms that feature significantly in the representation of the field increases in proportion to N.

Figure 3 shows portion of the dispersion relation near the Brillouin-zone boundary at $\hat{k}_x=1$, depicting interesting behavior of the IW and PIW there. The parameter values used in the calculation are $\nu=0.3$, $b/D=0.16$, $d/D=0$, and $N=47$. The figure also shows the thresholds T_0 and T_{-1}, and the $n=0$ L wave threshold L_0, which are independent of the value of b/D. The antisymmetrical field interfacial wave IW(A) persists down to $\hat{k}_x=0$, approaching asymptotically and degenerating with the T_0 threshold at this lower limit. For small b/D and away from $\hat{k}_x=0$ this mode takes on some of the features of the Rayleigh surface wave for each surface. This is supported by Fig. 4, which shows the variation of $V\beta=V/V_T$ with b/D for the various IW exactly at the zone boundary $\hat{k}_x=1$, where $V=\omega/k_x=\hat{\omega}/\hat{k}_x$ is the phase velocity along the surface. The limiting velocity of IW(A) as $b/D\rightarrow 0$ coincides with the Rayleigh surface wave velocity, which for $\nu=0.3$ is $V_R=0.9274V_T$.

The symmetrical field interfacial wave IW(S), as Fig. 4 shows, exists only for b/D below a critical value, which is ≈ 0.4 for $\nu=0.3$ and $d=0$, and slightly larger for small but finite d. Even where it does exist, it does not persist down to $k_x=0$ but degenerates with the T_0 threshold at a finite value of $\hat{k}_x$, which for $b/D=0.16$ is ≈ 0.7, as can be seen in Fig. 3.

The antisymmetrical pseudointerfacial wave PIW(A) lies a little below the T_{-1} threshold. It penetrates through the T_0 threshold and for a small range of $\hat{k}_x$ close to the zone boundary, it exists as a nonleaky proper interfacial wave IW(A′). Above the T_0 threshold it is able to absorb from and radiate into the T wave continuum, and it exists as a resonance rather than a true singularity. With decreasing $\hat{k}_x$, assuming $\beta/\alpha>\sqrt{2}$, which is the case for positive Poisson's ratio ν, this resonance becomes progressively narrower until at the intersection of the line $\hat{\omega}=\sqrt{2}\hat{k}_x$ with PIW(A), which corresponds to the incidence of a bulk T wave at an angle of $\pi/4$ to the surface, $\det(\tilde{M})$ vanishes identically, and PIW(A) exists at that point as a nonleaky secluded supersonic interfacial wave (SSIW).[36] This isolated IW comes about at the point where $\omega^2\beta^2=2(k_x^0)^2$, and hence, from Eq. (24) $\tilde{m}=0$, requiring [according to Eqs. (20) and (21)] either that $\tilde{A}_n=0$ and $\tilde{B}_n=\delta_{n0}$, or that $\det(\tilde{M})=0$. This implies the total decoupling of the interfacial wave from the bulk T wave continuum, rendering this mode a nonleaking proper IW.[37,38] At yet smaller values of $\hat{k}_x$, the SSIW reverts to being a PIW resonance with growing width as $\hat{k}_x$ is decreased. Eventually it crosses the L_0 threshold defined by $\hat{\omega}=(\beta/\alpha)\hat{k}_x$, which is accompanied by a further increase in the width of the resonance, due to the fact that there is now (in addition) the L wave continuum which the PIW is coupled into. It persists down to the center of the Brillouin zone, narrowing down again as $\hat{k}_x\rightarrow 0$, as will be discussed in Sec. V. The situation is different if $\beta/\alpha<\sqrt{2}$, which is the case when ν is negative, because now the L_0 threshold lies below the line $\hat{\omega}=\sqrt{2}\hat{k}_x$, and so what would have been the SSIW, lies within the L bulk wave continuum, to which it is coupled. In this case PIW(A) remains a resonance throughout, and this SSIW does not exist.

Figure 4, which is for $\nu=0.3$ and $\hat{k}_x=1$, pertains to standing modes with finite phase velocities but zero group velocities. The modes IW(S) and IW(A) both approach the Rayleigh velocity $V_R=0.9274V_T$ as $b/D\rightarrow 0$, i.e., as the bonded regions are shrunk to points.[39] In this limit they are both superpositions of oppositely traveling Rayleigh surface waves of wavelength $\lambda=2D$. The superposition can be such

that it results in nodal points for u_x or u_z but not simultaneously for both components of displacement. Specifically, in the case of IW(S), the nodal points are for u_z and occur at positions pD; $p=0,\pm 1,\pm 2,\ldots$, i.e., at the points where the two surfaces are joined. The u_x and u_z displacement components for a Rayleigh wave, as is well known,[25] are $\pi/2$ out of phase, and so this places the antinodes for u_x at the points of connection, which is consistent with the boundary conditions. In the case of IW(A), the situation is reversed, with the nodal points of u_x occurring at the points pD, where the surfaces are connected, while the antinodes for u_z occur at these points. The resonance frequency for these standing modes is

$$f_{\mathrm{res}} = 2V_R/D, \tag{26}$$

which could range from a few hundred hertz for mining stopes to many megahertz for submillimeter cracks.

As the value of b/D increases, these two standing modes become constrained, since in effect the nodal points become extended into nodal regions, and this shifts up their phase velocities and lifts their degeneracy. IW(S) increases more rapidly and ceases to exist at $b/D \approx 0.4$, when its phase velocity reaches V_T. IW(A) persists for all values of b/D but degenerates with T_0 as $b/D \to 1$. IW(A′) also exists for all b/D but with higher phase velocity than that of IW(A) throughout, and it approaches T_0 much earlier on. There is a fourth guided mode, IW(S′), which is not present in Fig. 3 because it exists only for a small range of b/D near zero, with its phase velocity being close to V_T.

IV. ROLE OF PSEUDOINTERFACIAL WAVES IN SCATTERING

Sharp features in the reflection and transmission coefficients for periodic arrays of cracks have been noted before in the literature,[3,5,7] and Danicki[7] attributed them to leaky interfacial waves but the subject has not been previously explored in any great depth. In this section we examine how these resonant features come about. The pseudointerfacial wave PIW(A) has a pronounced effect on the frequency dependence of the transmission and reflection of bulk waves at the interface, mainly brought about by the rapid variation of the phase of $\tilde{A}_0$ and $\tilde{B}_0$ for antisymmetrically incident L and T waves in the vicinity of this mode. Figures 5(a) and 5(b) show, respectively, plots, as a function of $\hat{\omega}/2$, of the absolute value of the reflection and transmission amplitude coefficients $|R_T^T| = |B_0 + \tilde{B}_0|/2$ and $|T_T^T| = |B_0 - \tilde{B}_0|/2$, respectively, for a T wave incident from one direction on the interface at an angle $\theta = 7\pi/24$. They have been calculated by decomposing this wave into symmetrically and antisymmetrically incident T waves, and the parameter values used are $\nu = 0.3$, $b/D = 0.5$, and $d/D = 0$. The angle of incidence is below the critical angle $\theta_c = \arccos(\alpha/\beta)$ for mode conversion to the bulk $n=0$ L wave. The insets of Figs. 5(a) and 5(b) are blowups of the region just beyond $\hat{\omega}/2 = 0.6$ where there is rapid variation in the scattering. The sharp peak at 0.6215 corresponds to the T_{-1} threshold. Below this value both B_0 and $\tilde{B}_0$ are in magnitude unity, since there is only one outgoing channel on each side of the interface into which they radiate, with the $n=0$ L modes being evanescent. The reflection and transmission amplitudes for the unidirectional T wave vary in this spectral range solely because of the variation of the phases of B_0 and $\tilde{B}_0$, which is depicted in Fig. 5(c). Well below the cutoff, the phase of $\tilde{B}_0$, starting off at $-\pi$, does not change much, while that of B_0, starting off from zero, increases steadily. The relative phase and its variation explain why $|R_T^T|$ starts off at zero and increases steadily, while $|T_T^T|$ starts off from unity and displays an increasing downward trend. Then, in the vicinity of PIW(A) the phase of $\tilde{B}_0$ undergoes a rapid increase through approximately 2π, and this causes $|R_T^T|$ to drop sharply to zero as the relative phase passes through π, to rise rapidly to unity as the relative phase passes through zero, and then level off, while $|T_T^T|$ undergoes similar sharp swings between the same two extremes but in the reverse order.

For comparison, Figs. 5(d) and 5(e) show, respectively, plots, as a function of $\hat{\omega}/2$, of the absolute value of the reflection and transmission coefficients for unidirectional T wave incident on the interface at the slightly smaller angle $\theta = \pi/4$, which is the condition for the perfect decoupling of the PIW from the $n=-1$ T bulk wave continuum and the existence of the SSIW. These curves are indistinguishable from results obtained by Mikata[5] for the same values of the parameters ($\hat{\omega}/2$ and b correspond, respectively, to the parameters $Dk_T/2\pi$ and $D-2a$). These curves are similar to the plots in Figs. 5(a) and 5(b) over most of the spectral range except in the vicinity of the PIW resonance, which is totally absent for $\theta = \pi/4$ because of the decoupling of PIW(A) from the continuum. It requires just the slightest deviation of the angle of incidence from $\theta = \pi/4$ to restore the PIW feature, initially as an extremely sharp resonance, and then broadening as the deviation of θ from $\pi/4$ increases.

Conservation of energy requires that the sum of the energy fluxes normal to the interface for all the outgoing homogeneous waves equals the energy flux normal to the interface for the incident wave. Right up to the T_{-1} threshold there are only the $n=0$ T reflection and transmission channels to radiate into, which requires therefore that $|R_T^T|^2 + |T_T^T|^2 = 1$. This condition is satisfied precisely by the scattering amplitudes portrayed in Fig. 5, providing a check on the validity of the method of this paper. Beyond the T_{-1} threshold, there is also the $n=-1$ T channel which to radiate into, and it has been verified here again that energy conservation is satisfied when that additional wave is included in the calculation and account is taken of the relevant angles. The sharp features at 0.874 in Figs. 5(a) and 5(b), and 0.805 in Figs. 5(d) and 5(e) occur at the L_{-1} threshold, beyond which the $n=-1$ L mode provides a further bulk wave radiation channel.

The PIW(A) also features, although not quite as prominently, in the transmission and reflection of L waves. Figure 6 shows the L wave reflection coefficient $|R_L^L|$ for a unidirectional L wave incident on the interface at an angle $\theta = \pi/4$, as a function of frequency in the spectral region of the PIW(A) and T_{-1}. The two curves correspond to different values of b/D but with the same $\nu = 0.3$ and $d/D = 0$. The curve for $b/D = 0.5$ coincides in this spectral region

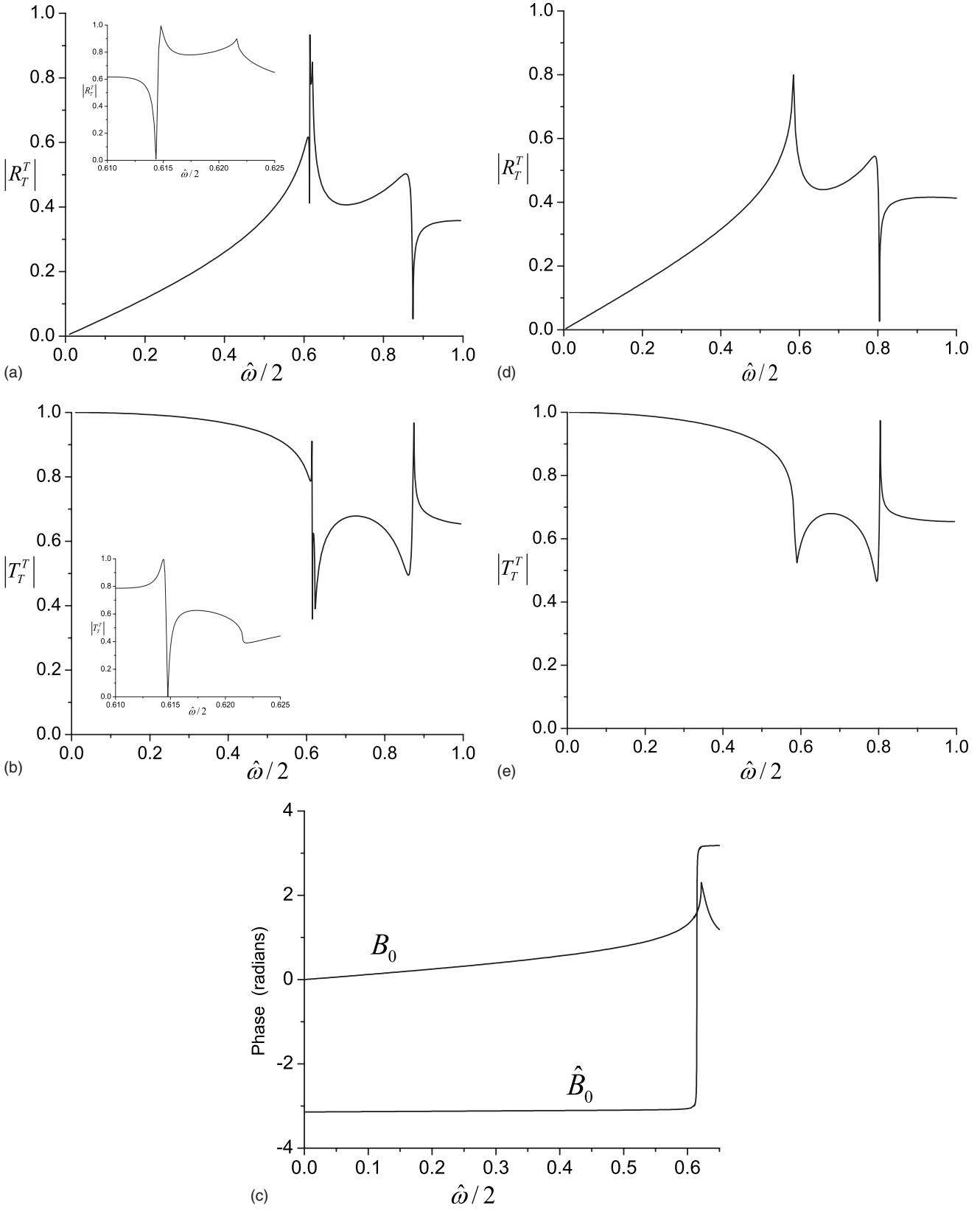

FIG. 5. (a) Reflection $|R_T^T|$ and (b) transmission $|T_T^T|$ amplitudes for T wave incidence at angle $\theta=7\pi/24$, with the parameter values being $\nu=0.3$, $b/D=0.5$, and $d/D=0$. The sharp peak at 0.6215 in the inset of (a) corresponds to the T_{-1} threshold, and the sharp resonance at about 0.6145, where $|R_T^T|$ and $|T_T^T|$ swing between 0 and 1 is the PIW(a). (c) Shows the phase variation of B_0 and $\tilde{B}_0$, which accounts for this behavior. (d) T wave reflection and (e) transmission for T wave incidence at angle $\theta=\pi/4$. The PIW(A) resonance is absent from these latter curves.

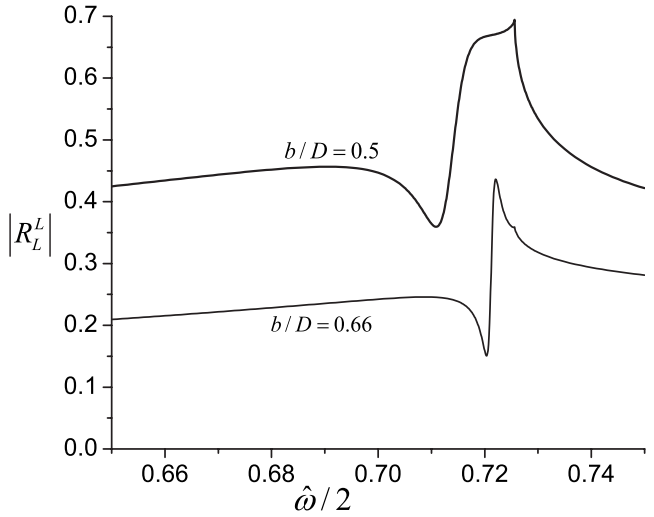

FIG. 6. L wave reflection amplitude $|R_L^L|$ for incidence angle $\theta=\pi/4$, $\nu=0.3$, and $d/D=0$, and two different values of b/D, restricted to the spectral region where the PIW(A) (the broad feature) and the T_{-1} threshold (the sharp feature) occur.

$0.65<\hat{\omega}/2<0.75$, with Fig. 3 of Mikata,[5] which was calculated for the equivalent parameter values. The sharp peaks in the two curves at $\hat{\omega}/2=0.726$ occurs at the T_{-1} threshold, and the more rounded feature of a dip followed by a rapid rise is associated with the PIW(A). With increasing value of b/D, i.e., greater degree of connection between the two solids, the interface is effectively stiffer,[27] and the overall reflectivity decreases, and the PIW(A) feature sharpens up and approaches the T_{-1} threshold, degenerating with it as $b/D\rightarrow 1$.

V. ZONE CENTER INTERFACIAL WAVES

Sections III and IV dealt with interfacial waves having wave vectors near the Brillouin-zone edge. There is also a system of interfacial waves near the zone center, which have a pronounced effect on the transmission and reflection of L and T waves at normal or near normal incidence. Danicki[7] drew attention to sharp resonances that occur in this situation, and in this section the dispersion relation for the IW that gives rise to these resonances is explored. For normal incidence and at frequencies below $T_{\pm 1}$, i.e., the point where the T_{-1} and T_{+1} thresholds intersect, there is no mode conversion between bulk L and T waves, and symmetric and antisymmetric mode features reveal themselves to be disentangled. Figure 7(a) pertains to an interface with $\nu=0.3$, $b/D=0.03$, and $d/D=0$, and shows the variation of the T wave reflection amplitude in the spectral region near $T_{\pm 1}$ for normal incidence ($\theta=\pi/2$) and incidence at a slight angle to normal ($\theta=\pi/2.03$). For normal incidence and below $T_{\pm 1}$, $|B_0|$ and $|\tilde{B}_0|$ are both unity, and the sharp dip to zero of $|R_T^T|$ at $\hat{\omega}/2=0.956$ is due to the phase of $|\tilde{B}_0|$ undergoing a swing through 2π. This phenomenon is associated with a PIW, labeled as PIW(A′), which (even at $\hat{k}_x=0$) is a resonance of finite width. At $\hat{k}_x=0$, $\tilde{M}$ also possesses a true singularity associated with a secluded SSIW at $\hat{\omega}/2=0.928$. When $\hat{k}_x$ deviates from zero, this mode becomes a PIW, labeled as PIW(A), allowing it to couple to T waves at non-normal incidence. This accounts for the narrow dip in the reflectivity at $\hat{\omega}/2=0.918$ for incidence at $\theta=\pi/2.03$.

Figure 7(b) reveals similar effects for L wave incidence, where it is the symmetric IW that are coupled to. It shows the L wave reflectivity $|R_L^L|$ in the same spectral region and values of the other parameters. For $\theta=\pi/2$, the sharp dip to zero at $\hat{\omega}/2=0.983$ is associated with a symmetric IW labeled PIW(S′) which (even at $\hat{k}_x=0$) is a resonance with finite width. At $\hat{k}_x=0$, M also possesses a true singularity associated with a secluded SSIW at $\hat{\omega}/2=0.928$. When $\hat{k}_x$ deviates from zero, this mode becomes a PIW, labeled as PIW(S), and this accounts for the narrow dip in the reflectivity at $\hat{\omega}/2=0.926$ for incidence at $\theta=\pi/2.03$.

Figure 8 shows portion of the dispersion relation for the above-mentioned PIW and the thresholds T_{-1} and T_{+1} for

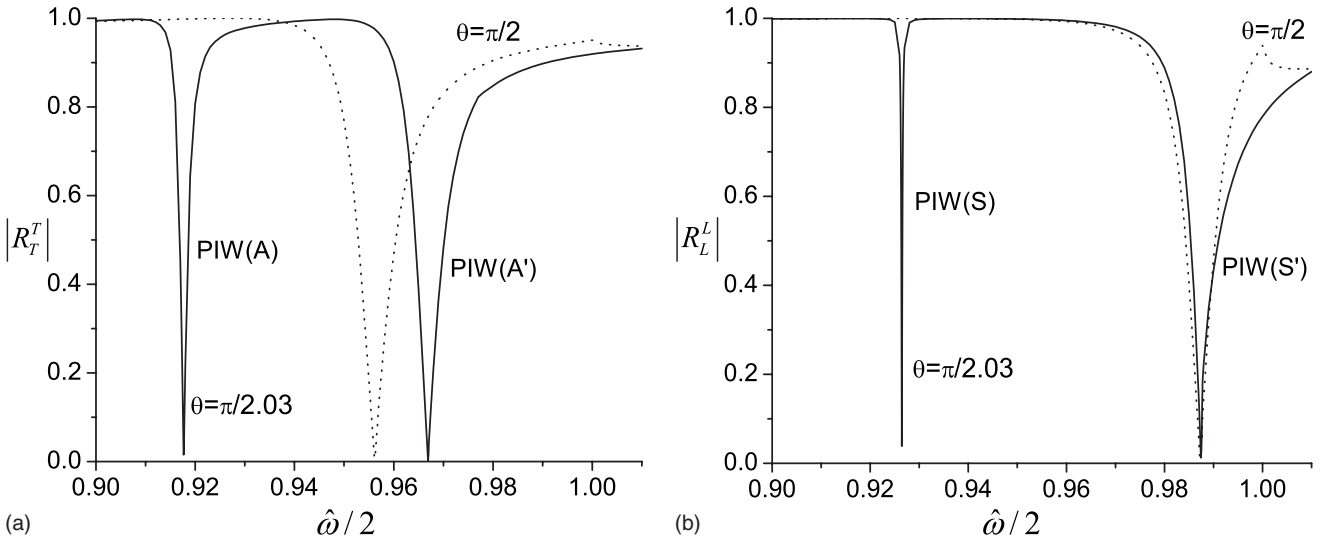

FIG. 7. Reflectivity for normal and near normal incidence in spectral region of PIW for $\nu=0.3$, $b/D=0.03$, and $d/D=0$. (a) $|R_T^T|$ and (b) $|R_L^L|$.

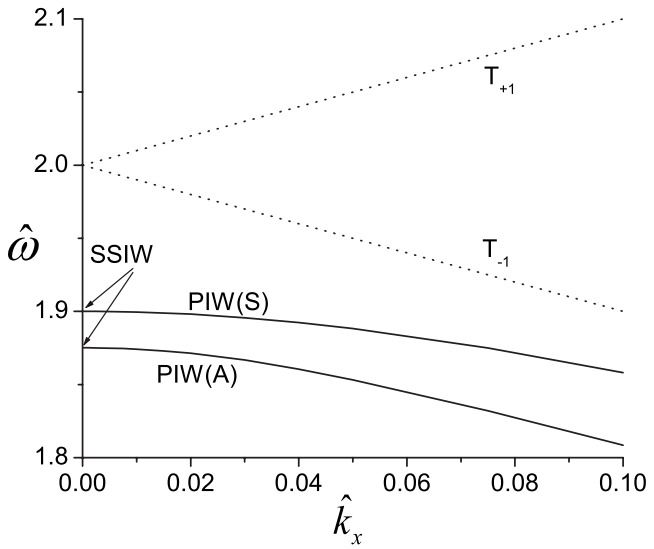

FIG. 8. Dispersion relation for the PIW near the Brillouin-zone center for $\nu=0.3$, $b/D=0.16$, and $d/D=0$. It shows also the thresholds T_{+1} and T_{-1}, which are independent of the value of b.

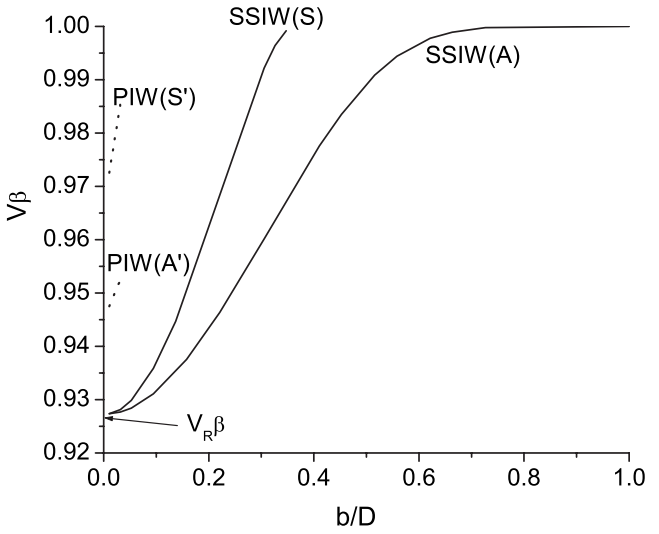

FIG. 9. Standing mode phase velocities at the zone center $\hat{k}_x=0$ as a function of b/D for $\nu=0.3$ and $d/D=0$.

$\nu=0.3$, $b/D=0.16$, and $d/D=0$. The modes PIW(S) and PIW(A) start off at $\hat{k}_x=0$ as SSIW, and with increasing $\hat{k}_x$ both curve downwards, becoming progressively broader PIW resonances as they do so. Much beyond $\hat{k}_x=0.1$, PIW(S) overlaps with T_{-1} and becomes difficult to follow. PIW(A) remains below T_{-1} and eventually toward the zone boundary becomes the mode identified as PIW(A) in Fig. 3.

Figure 9 shows the variation with b/D of $V\beta$ for the various IW, where $V=(\frac{\omega}{2\pi/D})$ is the effective phase velocity from taking $\hat{k}_x$ to be at the center of the second Brillouin zone. The limiting value of $V\beta$ for both PIW(A) and PIW(S) as $b/D \rightarrow 0$ is 0.9274, which identifies these modes as standing Rayleigh waves of wavelength $\lambda=D$, and with nodal points for u_x or u_z at the points where the two solids are joined. With increasing b/D, and hence, greater constraint, $V\beta$ for both of these modes increases. PIW(S) meets $T_{\pm 1}$ at $b/D=0.35$ and ceases to exist beyond that point, while PIW(A) degenerates with $T_{\pm 1}$ as $b/D \rightarrow 1$. PIW(A′) and PIW(S′) start off by showing an upward trend, but have broader features, which are more difficult to follow as they approach and overlap $T_{\pm 1}$.

VI. DISCUSSION

The numerical method used in this paper has been tested for values of N up to 67, and it is found to be numerically stable throughout this range and seemingly convergent with increasing N. This is no guarantee, of course, that the method is convergent in the strict mathematical sense. It may be that it is asymptotically divergent but nevertheless an accurate approximation for the larger values of N in the range we have considered. This notion was put forward by Maradudin and Zierau,[40] for instance, as a justification for their numerical treatment of surface waves at large amplitude sinusoidally corrugated surfaces. To be sure, by employing smoothly varying boundary conditions, the difficult and (to a large extent) unphysical singular behavior of the strain field often predicted by linear elasticity for the neighborhood of discontinuities in the boundary conditions has been avoided.[18] The method of the present paper is able to accurately reproduce the extensive set of transmission and reflection curves calculated by Mikata,[5] using a very different method, and this further supports its validity. Checks have also been carried out to confirm that energy conservation is satisfied by the bulk wave amplitudes emerging from the calculations.

The main findings of this paper pertain to the existence of a rich system of leaky and nonleaky interfacial waves at a periodic arrangement of thin coplanar cavities in a solid and to the striking influence of the pseudointerfacial waves on bulk wave scattering. The relationship of the interfacial waves to standing Rayleigh waves with wave vectors near the center and boundary of the first Brillouin zone has been explored.

ACKNOWLEDGMENTS

This project arose from discussions with R. J. Durrheim, S. M. Spottiswoode, and A. Milev on mine-induced seismicity. A. A. Maznev and A. L. Shuvalov are thanked for ongoing interest. The Laboratoire de Mecanique Physique, Université de Bordeaux 1 is thanked for hospitality. This work is based on research supported by the National Research Foundation and the Stellenbosch Institute for Advanced Study.

[1] J. D. Achenbach, *Wave Propagation in Elastic Solids* (North-Holland, Amsterdam, 1975).
[2] Y. C. Angel and J. D. Achenbach, ASME Trans. J. Appl. Mech. **52**, 33 (1985).
[3] Y. C. Angel and J. D. Achenbach, Wave Motion **7**, 375 (1985).
[4] Ch. Zhang, Int. J. Eng. Sci. **29**, 481 (1991).
[5] Y. Mikata, ASME Trans. J. Appl. Mech. **60**, 911 (1993).
[6] E. Danicki, J. Acoust. Soc. Am. **100**, 2942 (1996).
[7] E. J. Danicki, J. Acoust. Soc. Am. **105**, 84 (1999).
[8] E. J. Danicki, Wave Motion **35**, 355 (2002).
[9] D. A. Sotiropoulos and J. D. Achenbach, J. Acoust. Soc. Am. **84**, 752 (1988).
[10] G. A. Maugin, Y. Chevalier, and M. Louzar, Geophys. J. Int. **118**, 305 (1994).
[11] Y. Chevalier, M. Louzar, and G. A. Maugin, J. Acoust. Soc. Am. **98**, 445 (1995).
[12] M. Ciarletta and M. A. Sumbatyan, ASME Trans. J. Appl. Mech. **64**, 1004 (1997).
[13] Y. Mikata, ASME Trans. J. Appl. Mech. **62**, 312 (1995).
[14] Y.-S. Wang and D. Gross, Int. J. Solids Struct. **38**, 4631 (2001).
[15] Y. Mikata and J. D. Achenbach, Wave Motion **10**, 59 (1988).
[16] See, e.g., papers in the volume Z. Kristallogr. **220**, 9-10 (2005), which is devoted entirely to the subject of phononic crystals.
[17] See, e.g., papers on phononic crystals and scattering from corrugated surfaces in the programme of Acoustics'08, www.acoustics08-paris.org
[18] Divergence of the stress and strain fields, oscillatory singularities and material self intersection in the neighbourhood of boundary condition discontinuities, are some of the unphysical predictions of linear elasticity. See, e.g., A. R. Aguiar and R. L. Fosdick, Math. Models Meth. Appl. Sci. **10**, 1181 (2000); I. Simonov and K. Osipenko, Int. J. Fract. **116**, 297 (2002).
[19] J. R. Dutcher, S. Lee, B. Hillebrands, G. J. McLaughlin, B. G. Nickel, and G. I. Stegeman, Phys. Rev. Lett. **68**, 2464 (1992).
[20] L. Giovannini, F. Nizzoli, and A. M. Marvin, Phys. Rev. Lett. **69**, 1572 (1992).
[21] D. M. Profunser, O. B. Wright, and O. Matsuda, Phys. Rev. Lett. **97**, 055502 (2006).
[22] T. F. Crimmins, A. A. Maznev, and K. A. Nelson, Appl. Phys. Lett. **74**, 1344 (1999); A. A. Maznev, A. Mazurenko, L. Zhuoyun, and M. Gostein, Rev. Sci. Instrum. **74**, 667 (2003).
[23] Ch. Zhang, ASME Trans. J. Appl. Mech. **59**, 366 (1992).
[24] M. Caleap, C. Aristegui, and Y. C. Angel, J. Acoust. Soc. Am. **122**, 1876 (2007).
[25] J. L. Rose, *Ultrasonic Waves in Solid Media* (Cambridge University Press, Cambridge, 1999).
[26] K. Aki and P. G. Richards, *Quantitative Seismology* (University Science Books, Sausalito, 2002).
[27] J.-M. Baik and R. B. Thompson, J. Nondestruct. Eval. **4**, 177 (1984).
[28] A. I. Lavrentyev and S. I. Rokhlin, J. Acoust. Soc. Am. **103**, 657 (1998); W. Huang and S. I. Rokhlin, Geophys. J. Int. **118**, 285 (1994).
[29] V. Tvergaard and J. W. Hutchinson, J. Mech. Phys. Solids **40**, 1377 (1992).
[30] For the crack tip shape predicted on the basis of linear elasticity, see, e.g., M. Kachanov, B. Shafiro, and I. Tsukrov, *Handbook of Elasticity Solutions* (Kluwer, Dordrecht, 2003).
[31] S. Hirose and J. D. Achenbach, J. Acoust. Soc. Am. **93**, 142 (1993).
[32] C. Pecorari, J. Acoust. Soc. Am. **117**, 592 (2005).
[33] S. M. Spottiswoode, J. B. Scheepers, and L. Ledwaba, Proceedings of the SANIRE 2006 Facing the Challenges (South African National Institute of Rock Engineering, Rustenberg, South Africa, 2006), p. 140, http://www.sanire.co.za/member_pages/pdfs/Symp2006%20proceedings/index.php.
[34] J. D. Kaplunov (private communication), in unpublished calculations, has used the arctangent function for smoothing out boundary condition discontinuities.
[35] M. Castaings, E. Le Clezio, and B. Hosten, J. Acoust. Soc. Am. **112**, 2567 (2002).
[36] The analogous phenomenon for surfaces, that of secluded supersonic surface waves, has been studied by a number of authors, see e.g. S. A. Gundersen, L. Wang, and J. Lothe, Wave Motion **14**, 129 (1991); A. A. Maznev and A. G. Every, Phys. Lett. A **197**, 423 (1995).; They have been observed using surface Brillouin scattering, see, e.g., V. V. Aleksandrov, T. S. Velichkina, Ju. B. Potapova, and I. A. Yakovlev, Phys. Lett. A **171**, 103 (1991).
[37] A. A. Maznev (private communication) has drawn the author's attention to a related phenomenon, namely that for $\theta=\pi/4$ incidence of a SV wave on a free surface, there is no mode conversion to reflected L wave (Ref. 38).
[38] B. A. Auld, *Acoustic Fields and Waves in Solids* (Krieger, Malabar, 1990), Vol. II, pp. 30–35.
[39] D. V. Evans and R. Porter, Wave Motion **45**, 745 (2008) have treated the somewhat analogous situation of standing edge waves in a thin semi-infinite plate which is pinned at a periodic set of points at its edge.
[40] A. A. Maradudin and W. Zierau, Geophys. J. Int. **118**, 325 (1994).